Entanglement properties of a measurement-based entanglement distillation experiment

Hao Jeng,[1] Spyros Tserkis,[2] Jing Yan Haw,[1] Helen M. Chrzanowski,[1,3] Jiri Janousek,[1] Timothy C. Ralph,[2] Ping Koy Lam,[1] and Syed M. Assad[1,*]

[1]*Centre for Quantum Computation and Communication Technology, Research School of Physics and Engineering, The Australian National University, Canberra, Australian Capital Territory 2601, Australia*

[2]*Centre for Quantum Computation and Communication Technology, School of Mathematics and Physics, University of Queensland, St. Lucia, Queensland 4072, Australia*

[3]*Institute of Physics, Humboldt-Universität zu Berlin, Newtonstr. 15, D-12489 Berlin, Germany*

(Received 15 November 2018; published 1 April 2019)

Measures of entanglement can be employed for the analysis of numerous quantum information protocols. Due to computational convenience, logarithmic negativity is often the choice in the case of continuous-variable systems. In this work, we analyze a continuous-variable measurement-based entanglement distillation experiment using a collection of entanglement measures. This includes logarithmic negativity, entanglement of formation, distillable entanglement, relative entropy of entanglement, and squashed entanglement. By considering the distilled entanglement as a function of the success probability of the distillation protocol, we show that the logarithmic negativity surpasses the bound on deterministic entanglement distribution at a relatively large probability of success. This is in contrast to the other measures which would only be able to do so at much lower probabilities, hence demonstrating that logarithmic negativity alone is inadequate for assessing the performance of the distillation protocol. In addition to this result, we also observed an increase in the distillable entanglement by making use of upper and lower bounds to estimate this quantity. We thus demonstrate the utility of these theoretical tools in an experimental setting.

DOI: 10.1103/PhysRevA.99.042304

I. INTRODUCTION

On the one hand, quantum entanglement is a useful nonclassical resource. It can be used for the construction of quantum gates [1] or for the distribution of cryptographic keys in a secure manner [2]. On the other hand, implementations of these tasks are usually limited in performance due to experimental imperfections. Utilizing a variety of methods such as photon subtraction [3,4] and noiseless linear amplification [5,6], entanglement distillation protocols seek a potential resolution to this problem by concentrating weakly entangled states into subsets that are more entangled.

Here we address the problem of quantifying entanglement distillation; this will, in general, depend on the kind of system that one is working with. In the case of discrete variables, the fidelity with respect to some maximally entangled state [7] and nonlocality based on the Bell inequalities [8] are both useful measures for observing quantum entanglement. However, these methods are not particularly suitable in the case of continuous variables. Maximally entangled continuous-variable states are unphysical, and a theorem from Bell precludes the demonstration of nonlocality using Gaussian states and Gaussian measurements (the standard tools for continuous variable experiments) [9], unless one introduces additional assumptions on one's system [10,11]. Thus far, the analyses of continuous-variable entanglement distillation have instead centered around inseparability criteria [12,13] and, most notably, the logarithmic negativity [14] as one can calculate it quite straightforwardly.

In this work, we analyze a continuous-variable measurement-based entanglement distillation experiment [5] using a collection of measures. We present two main results. First, we show that the logarithmic negativity is distinct from the other measures; it crosses the "deterministic bound" before the other measures do, at a probability of success (of the distillation protocol) that is orders of magnitude greater. The deterministic bound is the maximum entanglement that can be deterministically distributed across a given quantum channel (usually imperfect), assuming that one had an Einstein-Podolsky-Rosen (EPR) resource state with infinite squeezing. For instance, when the entanglement of formation crosses this bound, we can take it to indicate a form of error correction [15], thus giving an example of how the logarithmic negativity can fail to capture important properties of distillation protocols. Our results can be regarded as an experimental demonstration of such an example.

Our second result is the certification of an increase in the distillable entanglement. Currently, there is no known way to evaluate the distillable entanglement directly, which means that one is only able to look at it through the use of upper and lower bounds [16,17]. The upper bound puts a limit on how much distillable entanglement we had prior to distillation, while the lower bound guarantees at least how much we have after performing distillation. By observing a sufficient increase in the lower bound, we could certify that the distillable entanglement has indeed increased. We remark that the minimization of optical loss and the choice

*cqtsma@gmail.com

of a sharp upper bound turned out to be important factors in order to observe the increase in the distillable entanglement. In particular, there are many possible choices for the upper bound, but the relative entropy of entanglement was found to be the only one that was sufficiently stringent for this task.

We have organized this paper as follows. In Sec. II, we provide some background in Gaussian quantum optics and establish the notations and conventions that will be used throughout this paper. In Sec. III, definitions of the various entanglement measures are provided, discussing their basic properties with an emphasis on operational interpretations. In Sec. IV, the final section, we briefly describe the experiment setup and present a discussion of the distillation results based on the measures.

II. PRELIMINARIES

Gaussian states can be characterized by the first and second moments of the quadrature operators [18]—also known respectively as the mean fields and the covariance matrix. Since measures of entanglement depend only on the covariance matrix, we will assume vanishing mean fields without the loss of generality. For two-mode Gaussian states, the covariance matrix can be written in block form (using the $xpxp$ notation [19]):

$$\sigma = \begin{bmatrix} M & C \\ C^T & N \end{bmatrix},$$

where M, N, and C are real 2×2 matrices. In general, the entries of the covariance matrix depend on the value of $\hbar$; in this paper, we will normalize to the variance of the vacuum field, which amounts to setting $\hbar = 2$. In order for the covariance matrix to represent a physical state, it is also required to satisfy the Heisenberg uncertainty principle.

The density matrix of closed quantum systems evolve under unitaries: $\hat{\rho} \to \hat{U}\hat{\rho}\hat{U}^\dagger$. In general, representations of these unitaries in the Fock basis require infinite-dimensional matrices; if we restrict ourselves to Gaussian operations, then this can be simplified to the evolution of covariance matrices: $\sigma \to S\sigma S^T$. For two-mode states, each S is a 4×4 square matrix and is symplectic with respect to the following symplectic form:

$$\Omega = \begin{bmatrix} 0 & 1 & 0 & 0 \\ -1 & 0 & 0 & 0 \\ 0 & 0 & 0 & 1 \\ 0 & 0 & -1 & 0 \end{bmatrix}.$$

It satisfies the equation $S\Omega S^T = \Omega$. Every Gaussian unitary $\hat{U}$ is associated with a symplectic matrix. We will find the following unitary useful:

$$\hat{S}_2(r) = e^{r(\hat{a}\hat{b} - \hat{a}^\dagger \hat{b}^\dagger)/2}, \tag{1}$$

which is known as the two-mode-squeezing operator. As usual, $\hat{a}$ and $\hat{b}$ denote the annihilation operators of the two optical modes. The two-mode-squeezing operator is parametrized by the squeezing parameter r, with $r = 0$ corresponding to no squeezing and $r \to \infty$ to the limit of infinite squeezing.

Any given covariance matrix σ can be put into the following standard form:

$$\sigma = \begin{bmatrix} m & 0 & c_1 & 0 \\ 0 & m & 0 & c_2 \\ c_1 & 0 & n & 0 \\ 0 & c_2 & 0 & n \end{bmatrix}, \tag{2}$$

and this can be done using only local Gaussian unitaries [13], which does not change the entanglement of the state.

One can always diagonalize the covariance matrix using only symplectic matrices, and the corresponding eigenvalues are called symplectic eigenvalues [20]. Of particular importance are the symplectic eigenvalues of the partially transposed state. For two-mode Gaussian states, the partial transpose flips the sign of the phase quadrature, equivalent to flipping the sign of the c_2 entry in the standard form of the covariance matrix [Eq. (2)]. The symplectic eigenvalues $\tilde{\nu}_\pm$ of the partially transposed state are given by

$$\tilde{\nu}_\pm^2 = \frac{\tilde{\Delta} \pm \sqrt{\tilde{\Delta}^2 - 4 \det \sigma}}{2}, \tag{3}$$

where $\tilde{\Delta} = \det M + \det N - 2 \det C$.

For convenience, covariance matrices of the form

$$\sigma = \begin{bmatrix} m & 0 & c & 0 \\ 0 & m & 0 & -c \\ c & 0 & m & 0 \\ 0 & -c & 0 & m \end{bmatrix} \tag{4}$$

will be called symmetric, while those of the form

$$\sigma = \begin{bmatrix} m & 0 & c & 0 \\ 0 & m & 0 & -c \\ c & 0 & n & 0 \\ 0 & -c & 0 & n \end{bmatrix} \tag{5}$$

will be called quadrature symmetric. These states form strict subsets of general two-mode Gaussian states [Eq. (2)] by imposing different kinds of symmetries.

III. ENTANGLEMENT MEASURES

We present some background on the theory of entanglement measures, including definitions, properties, and formulas that will be useful. We note that the problem of computing entanglement measures is NP-complete for many measures [21], with analytical expressions available only in restricted cases that will generally possess some degree of symmetry. In the special case of the entanglement of formation, such a restriction will give rise to a simple operational interpretation in terms of quantum squeezing and thus a connection to the logarithmic negativity which we briefly discuss.

A. Entanglement entropy

The entanglement entropy $\mathcal{E}_V$ uniquely determines entanglement on the set of pure states. Given the von Neumann entropy S, with

$$S(\hat{\rho}) = -\mathrm{tr}(\hat{\rho} \ln \hat{\rho}), \tag{6}$$

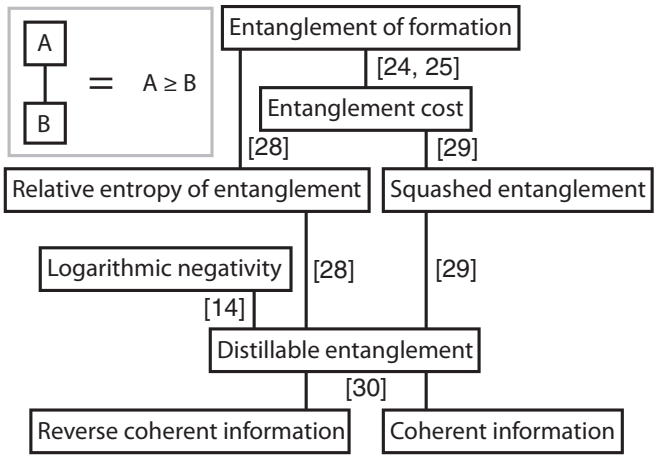

FIG. 1. An ordering of the measures. If a measure A sits above B with a line connecting them, then $A(\hat{\rho}) \geqslant B(\hat{\rho})$ for all states $\hat{\rho}$. If one considers only pure states, then all measures shown in the diagram (except the logarithmic negativity) reduce to the entanglement entropy. When restricting to pure two-mode Gaussian states, the logarithmic negativity and the entanglement entropy can also be regarded as equivalent in the sense of Eq. (13). Citations in the figure refer to proofs for each inequality.

the entanglement entropy $\mathcal{E}_V$ is defined to be the von Neumann entropy of the reduced states [22]:

$$\mathcal{E}_V(|\psi\rangle) = S(\hat{\rho}_A) = S(\hat{\rho}_B). \tag{7}$$

The subscripts A and B denote the two subsystems of $|\psi\rangle$: $\hat{\rho}_A = tr_B(|\psi\rangle\langle\psi|)$ and $\hat{\rho}_B = tr_A(|\psi\rangle\langle\psi|)$. For Gaussian states, the von Neumann entropy depends only on the symplectic eigenvalues of the covariance matrix.

B. Entanglement cost and distillable entanglement

The extension of the entanglement entropy to mixed states is not unique. Two possible choices are the entanglement cost and the distillable entanglement; they are quite fundamental, since they represent, respectively, the average pure state entanglement that is needed for or that can be extracted from any given state (usually mixed). The precise definitions are quite cumbersome to state and somewhat unnecessary for this paper, but they can be found in, for instance, Horodecki *et al.* [23]. The entanglement cost is an upper bound to the distillable entanglement (Fig. 1), and they both reduce to the entanglement entropy on the set of pure states. Neither measure is straightforward to compute in general.

The entanglement cost is the asymptotic (regularized) version of the entanglement of formation [24], the latter of which can be computed for two-mode Gaussian states and is discussed in the next subsection. It follows from this regularization formula (and the subadditivity of the von Neumann entropy) that the entanglement of formation bounds the entanglement cost from above [24,25]; in fact, recent work shows that the two quantities coincide on a subset of states [26], but the extent to which their equivalence holds is presently unknown.

The distillable entanglement, on the other hand, does not admit any closed expressions that we can evaluate straightforwardly. It can be upper bounded by a number of quantities (see Fig. 1): the entanglement of formation [27], the relative entropy of entanglement [28], the squashed entanglement [29], and the logarithmic negativity [14]; it also admits lower bounds due to the coherent and reverse coherent information [30]. We shall find such bounds useful for estimating the distillable entanglement.

C. Entanglement of formation

The entanglement of formation measures the minimum cost for producing a state starting from pure entanglement resources [27]:

$$\mathcal{E}_F(\hat{\rho}) = \inf\left\{\sum_j p_j \mathcal{E}_V\left(|\psi_j\rangle\right) \mid \hat{\rho} = \sum_j p_j |\psi_j\rangle\langle\psi_j|\right\}, \tag{8}$$

where $\mathcal{E}_V$ is the entanglement entropy. The infimum runs over all physical decompositions, including those that involve non-Gaussian states; however, the minimum is attained by Gaussian states if $\hat{\rho}$ is a two-mode Gaussian state [31,32]. This result also implies the equivalence between the entanglement of formation and the *Gaussian* entanglement of formation for two-mode Gaussian states.

Unlike logarithmic negativity, the optimization required by the entanglement of formation makes computation difficult [33,34]. A simple operational interpretation of the entanglement of formation manifests when one restricts attention to quadrature-symmetric states [35], allowing one to interpret it as the squeezing operations required to produce the state. Concretely, if σ is a two-mode Gaussian state taking the form of Eq. (5), then the entanglement of formation of σ is given by the following analytic expression:

$$\mathcal{E}_F(\sigma) = \cosh^2 r_0 \ln(\cosh^2 r_0) - \sinh^2 r_0 \ln(\sinh^2 r_0), \tag{9}$$

where

$$r_0 = \frac{1}{2}\ln\sqrt{\frac{\kappa - \sqrt{\kappa^2 - \lambda_+\lambda_-}}{\lambda_-}}, \tag{10}$$

with $\kappa = 2(\det\sigma + 1) - (m-n)^2$ and $\lambda_\pm = \det M + \det N - 2\det C + 2[(mn + c^2) \pm 2c(m+n)]$. The meaning of r_0 is depicted in Fig. 2—it can be identified as the minimum amount of two-mode squeezing that is needed to produce the state σ, corresponding to an optimal choice of the separable resource. For general two-mode Gaussian states, the expression [Eqs. (9) and (10)] is a lower bound on the entanglement of formation and lies relatively close to the exact value [35].

The symmetry requirements of Eqs. (9) and (10) are, fortunately, not too stringent; for instance, the standard protocols of entanglement swapping [36] and entanglement-based quantum key distribution [37] work with entangled resources of this type. However, experimental implementations of these protocols will necessarily be imperfect, which means that quantum states produced in the laboratory are never perfectly symmetrical. In such cases, numerical methods for calculating the entanglement of formation of arbitrary two-mode Gaussian states can be quite useful [34,38,39].

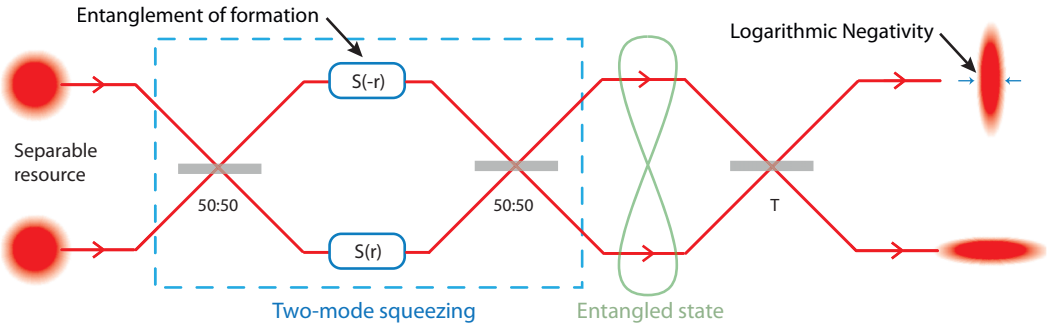

FIG. 2. A comparison of the logarithmic negativity (equivalently, the PPT criterion) and the entanglement of formation. The operational interpretations of the two measures can be illustrated in terms of quantum squeezing, and the picture above holds for two-mode Gaussian states that are symmetric in quadratures [those represented by Eq. (5)]. The minimum two-mode squeezing required to produce the entangled state corresponds to the entanglement of formation, while the maximum local squeezing that can be extracted from the entangled state can be identified with the symplectic eigenvalue $\tilde{\nu}_-$ and hence with the logarithmic negativity as well. The decomposition of two-mode squeezing into single-mode squeezers and passive operations has been shown explicitly; in addition, the beam-splitting ratio T that achieves maximal local squeezing will, in general, be state dependent. The separable resource need not be symmetric [i.e., of the form in Eq. (4)] if the entangled state is not and can also support nonvanishing correlations across the two modes as long as it remains separable.

D. Logarithmic negativity

For arbitrary density matrices $\hat{\rho}$, the logarithmic negativity $\mathcal{E}_N$ is defined to be [14]

$$\mathcal{E}_N(\hat{\rho}) = \ln ||\hat{\rho}^{\mathrm{PT}}||_1. \tag{11}$$

The symbol $||\cdot||_1$ denotes the trace norm, the notation PT is shorthand for the partial transpose. For two-mode Gaussian states σ, the logarithmic negativity is a simple function of the symplectic eigenvalue of the partially transposed state $\tilde{\nu}_-$:

$$\mathcal{E}_N(\sigma) = \begin{cases} 0, & \text{if } \sigma \text{ is separable} \\ -\ln \tilde{\nu}_-, & \text{otherwise} \end{cases}. \tag{12}$$

It is thus a good indicator of inseparability by virtue of the positive partial transpose (PPT) criterion [40,41], which states that a Gaussian state is separable if and only if $\tilde{\nu}_- \geqslant 1$ [12]. The logarithmic negativity coincides with the exact PPT-entanglement cost [42].

While the symplectic diagonalization of two-mode Gaussian states will lead to uncorrelated thermal states, the symplectic diagonalization of its partial transpose will lead to squeezing. It is easy to see that the maximum amount of local squeezing one can obtain from a two-mode Gaussian state is given by the symplectic eigenvalue of its partial transpose $\tilde{\nu}_-$ and that this can be achieved by interfering the two modes on a beamsplitter (Fig. 2). Although it does not hold in the most general case of Eq. (2), it does hold up to states with the symmetries of Eq. (5). As a consequence of this operational interpretation for $\tilde{\nu}_-$, it is related to the entanglement of formation through the following inequality [Ref. [39], Eq. (43)]:

$$\tilde{\nu}_- \geqslant e^{-2r_0}, \tag{13}$$

which essentially expresses the conservation of squeezing. The equality is attained by symmetric states, but the two measures are in general not equivalent. It has also been conjectured that e^{-2r_0} is bounded from below by some nontrivial function of $\tilde{\nu}_-$ [39], and the gap between the upper and lower bounds would imply that the two measures do not impose the same ordering on quantum states. The disagreement of measures on the ordering of states holds quite generally for the other entanglement measures as well [43].

E. EPR steering

By performing measurements of different observables on one party of an entangled state, it is possible to steer the other party into different types of quantum states [44–46]. In continuous-variable quantum optics, EPR steering can occur when any of the following inequalities on the conditional variances is violated [47]:

$$\mathcal{E}_{A>B} = V_{x_B|x_A} V_{p_B|p_A} \geqslant 1,$$
$$\mathcal{E}_{B>A} = V_{x_A|x_B} V_{p_A|p_B} \geqslant 1.$$

The symbol $V_{x_A|x_B}$ denotes the conditional variance of the quadrature $\hat{x}_A$ given $\hat{x}_B$, with the other quantities interpreted in a similar fashion. The subscripts A and B denote two parties sharing a bipartite entangled state. Two inequalities instead of one is necessary for describing steering, because it is a directional quantity. If we assume, without the loss of generality, that entanglement is generated by the party A and distributed to the party B, then we call $\mathcal{E}_{A>B}$ forward steering and $\mathcal{E}_{B>A}$ reverse steering. The party that performs the measurement is the party that performs steering; that would be A in the case of $\mathcal{E}_{A>B}$ and B in the case of $\mathcal{E}_{B>A}$. It is possible for a quantum state to be steerable in one direction but not in the other. In this case, only one of the inequalities above is violated.

EPR steering is not a measure of entanglement, since it does not characterize the separability of quantum states [48–50]. It is a sufficient condition for inseparability but not a necessary condition—there exists quantum states that are entangled but not steerable in either direction. We note that EPR steering has found applications in quantum key distribution—in particular, one-sided device-independent quantum key distribution [51,52]—where the secure keyrate turned out to be a simple function of EPR steering.

F. Relative entropy of entanglement

The quantum relative entropy between any pair of density operators $\hat{\rho}$ and $\hat{\sigma}$ is defined to be

$$S(\hat{\rho}||\hat{\sigma}) = \mathrm{tr}\hat{\rho}(\ln\hat{\rho} - \ln\hat{\sigma}). \tag{14}$$

The relative entropy of entanglement of $\hat{\rho}$ is then defined by minimizing the relative entropy over separable states [50]:

$$\mathcal{E}_R(\hat{\rho}) = \inf_{\hat{\sigma}\ \text{separable}} S(\hat{\rho}||\hat{\sigma}). \tag{15}$$

By construction, it is zero if and only if $\hat{\rho}$ is separable. The relative entropy of entanglement is an upper bound to the distillable entanglement and a lower bound to the entanglement of formation [28]. One can further specialize the domain of optimization to Gaussian states, leading to the Gaussian relative entropy of entanglement [53,54]:

$$\mathcal{E}_{\mathrm{GR}}(\hat{\rho}) = \inf_{\substack{\hat{\sigma}\ \text{separable}\\ \hat{\sigma}\ \text{Gaussian}}} S(\hat{\rho}||\hat{\sigma}). \tag{16}$$

The separable state which achieves the minimum of Eq. (15) is called the closest separable state, and can be non-Gaussian even if $\hat{\rho}$ is Gaussian [55]; hence, the relative entropy of entanglement and its Gaussian approximation are not equivalent.

One does not have closed expressions for the relative entropy of entanglement in general [56]. Although there are numerical methods based on semidefinite programming [57], this technique is ill suited in terms of computational time and memory requirements for continuous-variable systems; in this paper, we will simply use the Gaussian relative entropy of entanglement as an approximation. We show that the approximation is good in the regime that we care about. Finally, we note that the relative entropy of entanglement has been applied to the study of quantum repeaters; it is an upper limit on the channel capacity, when one does not have access to a quantum repeater [58].

G. Squashed entanglement

Squashed entanglement is a measure based on the conditional mutual information [29]:

$$\mathcal{E}_{\mathrm{sq}}(\hat{\rho}_{AB}) = \frac{1}{2}\inf_{\hat{\rho}_{ABE}} I(A:B|E), \tag{17}$$

where one tries to minimize the conditional mutual information $I(A:B|E) = S(\hat{\rho}_{AE}) + S(\hat{\rho}_{BE}) - S(\hat{\rho}_E) - S(\hat{\rho}_{ABE})$ over all purifications $\hat{\rho}_{ABE}$ of the bipartite state $\hat{\rho}_{AB}$. The subscripts A, B, and E denote the corresponding subsystems similar to that in Eq. (7). The optimization is difficult to perform, but one can exploit clever choices of the purification to obtain bounds on the squashed entanglement [59]. Like the relative entropy of entanglement, squashed entanglement is a bound on the capacities of quantum communication channels; furthermore, it satisfies many axioms of entanglement theory that other measures do not [60].

H. Coherent information

The coherent [61] and reverse coherent information [62,63] are defined as

$$I_C(\hat{\rho}) = S(\mathrm{tr}_A\hat{\rho}) - S(\hat{\rho}), \tag{18}$$

$$I_{\mathrm{RC}}(\hat{\rho}) = S(\mathrm{tr}_B\hat{\rho}) - S(\hat{\rho}), \tag{19}$$

and, as usual, the A and B subscripts denote subsystems of the bipartite state $\hat{\rho}$. These two measures are not entanglement measures in the axiomatic sense [50]; however, they satisfy the hashing inequality [30,58]:

$$\max(I_C(\hat{\rho}), I_{\mathrm{RC}}(\hat{\rho})) \leqslant \mathcal{E}_D(\hat{\rho}), \tag{20}$$

where $\mathcal{E}_D$ denotes the distillable entanglement. By virtue of the hashing inequality, the coherent and reverse coherent information provide sufficient conditions for inseparability and play the role of a lower bound in characterizing communication channels [58]. This is in contrast to the relative entropy of entanglement and squashed entanglement, which would both correspond to upper bounds.

To conclude this section, we emphasize that we have made a choice to work with one particular type of quantum correlation—namely quantum entanglement. It is a suitable choice for the analysis of entanglement distillation which we present in the next section. Other interesting options include discord measures [64], a measure of squeezing [65], and coherence measures [66]; however, we will not attempt to pursue these directions here.

IV. EXPERIMENT

A. Entanglement generation and processing

We study measurement-based distillation of quantum entanglement using recent advances in entanglement theory. The experiment setup (Fig. 3) consisted of a pair of bow-tie optical parametric amplifiers driven at 532 nm, with bright squeezed light generated at 1064 nm. The two beams were combined on a balanced beamsplitter, with a relative phase of $\pi/2$ to give Einstein-Podolsky-Rosen entanglement. One mode of this EPR pair was sent through a communication channel. Under the assumption that the quantum state is Gaussian, we can describe the state using just the first and second moments; five hundred sets of two million optical quadrature measurements were collected from each homodyne detector, retaining the 3- to 4-MHz narrowband through digital high-pass and low-pass filtering. Measurement-based entanglement distillation was performed using an approach similar to Ref. [5], by postprocessing the homodyne measurement data.

In practice, the communication channel through which we distribute the entanglement will be lossy; here we will assume that the loss is entirely passive and model it as a beamsplitter with fixed transmissivity. This was implemented using a polarizing beamsplitter preceeded by a half-wave plate. As we vary the loss, we can compare the logarithmic negativity and the entanglement of formation using the *effective squeezing*, which varied according to Fig. 4. We use the term "effective squeezing" of the logarithmic negativity and the entanglement of formation to refer to the quantities $\tilde{\nu}_-$ and $\exp(-2r_0)$, respectively. These quantities characterize the respective

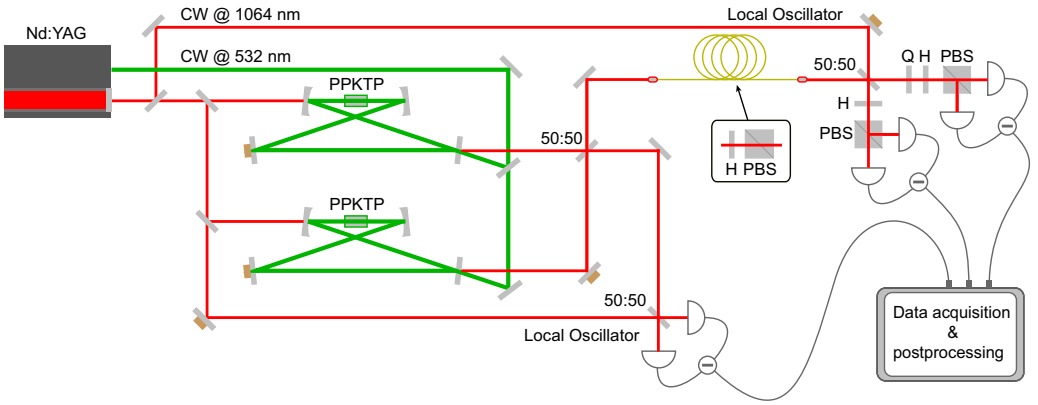

FIG. 3. Schematic of the measurement-based noiseless linear amplification (MBNLA) experiment [5]. Squeezed states were generated from a pair of bow-tie cavities using the optical $\chi^{(2)}$ nonlinearity and combined on a balanced beamsplitter to generate Einstein-Podolsky-Rosen entanglement. One of the beams from the EPR is sent through a communication channel that has optical loss, while the other is sent to a homodyne for verification; the transmission of the channel was characterized by optical heterodyne detection. Postprocessing was applied on the data collected from the homodynes to emulate noiseless linear amplification and thus the distillation of entanglement. H, half-wave plate; Q, quarter-wave plate; PBS, polarizing beamsplitter; CW, continuous wave; PPKTP, periodically poled potassium titanyl phosphate.

measures and, at the same time, can be interpreted as quantum squeezing (Secs. III C and III D.) At unity transmissivity (no loss), the state is symmetric but mixed, due to decoherence in the entanglement generation process. Despite the mixture, the measures remain equivalent due to the symmetry. In the presence of loss, the states are asymmetric and the measures are no longer equal. This is with the exception of maximal loss (zero transmissivity), where nothing is transmitted and the state is separable. All measures register effectively no squeezing in this case, which corresponds to unity when expressed as a variance.

The effects of passive loss can be mitigated through the use of noiseless linear amplification (NLA) [67,68]. This peculiar

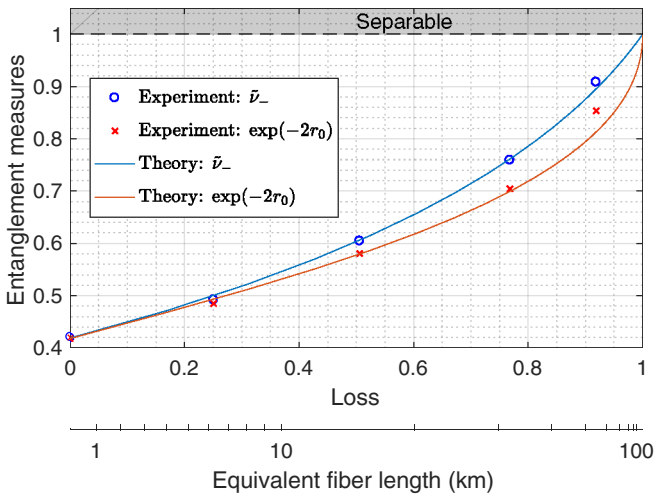

FIG. 4. Distribution of an entangled state through channels with various amounts of optical loss. Circles and crosses are from experiments, solid lines are theory, and the shaded region above the dashed line correspond to separable states. We include a meter below the figure, which gives the loss-equivalent distance assuming telecom wavelength (i.e., 1550 nm), with the ticks distributed according to a logarithmic scale.

amplifier can be described by an unbounded operator $g^{\hat{n}}$, where g represents the amplitude gain. Acting the noiseless linear amplifier on a coherent state will amplify the complex amplitude without increasing the noise, while acting it on a continuous-variable EPR state with loss would lead to a state with increased squeezing and reduced loss [67]. Due to the unbounded nature of the NLA operator, implementations are necessarily approximate; in order to avoid violating the Heisenberg uncertainty principle, they must also be nondeterministic [69]. Experimental implementations of the NLA are subject to additional limitations, such as restrictions on the size of the input coherent amplitudes to small values [70].

In this paper, a virtual implementation of the noiseless linear amplifier [5] has been chosen due to the ease of implementation. An NLA followed by optical heterodyning is equivalent to heterodyning followed by data processing; thus one is able to implement the noiseless linear amplifier in the form of data processing, provided that one performs a heterodyne measurement. Concretely, one takes each outcome α of the heterodyne and postselects it with an acceptance probability given by [71]:

$$P(\alpha) = \begin{cases} e^{(1-1/g^2)(|\alpha|^2-|\alpha_c|^2)}, & |\alpha| \leqslant |\alpha_c| \\ 1, & |\alpha| > |\alpha_c| \end{cases}, \qquad (21)$$

where g corresponds to the amplitude gain and α_c is a constant which specifies a cutoff. One then scales the successful events by multiplication: $\alpha \mapsto \alpha/g$. The postselection and rescaling make up the data-processing stage which emulates the noiseless linear amplifier. The closeness by which this measurement-based implementation approximates the true NLA depends on the cutoff—a larger cutoff will improve the approximation at the expense of a smaller probability of success [72].

B. Experiment analysis

The results of the analysis is presented in Figs. 5, 6, and 8. We considered three different settings of loss—90% [Figs. 5(a), 5(b), and 8(a)], 50% [Fig. 8(b) and 8(c)], and

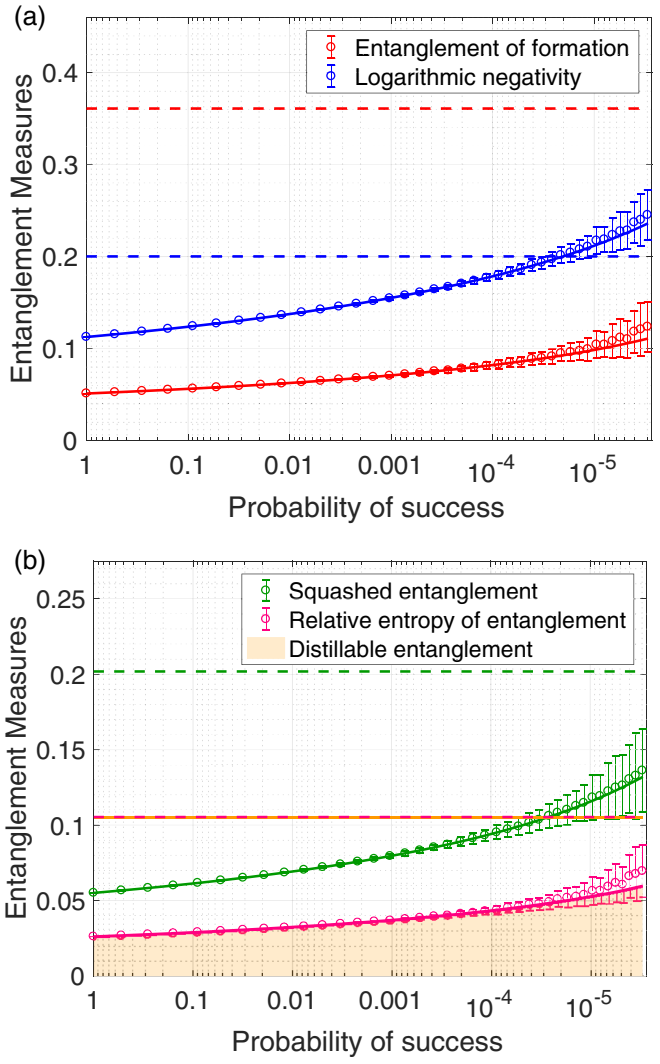

FIG. 5. Entanglement measures as a function of the probability of success. The optical loss was set to 90%. Circles correspond to experiment data (from top: logarithmic negativity, entanglement of formation, squashed entanglement, relative entropy of entanglement), solid lines to theory calculations, dashed lines to the (measure-dependent) deterministic bound (from top: entanglement of formation, logarithmic negativity, squashed entanglement, relative entropy of entanglement and distillable entanglement superimposed), and error bars represent 1.5 standard deviations over 100 repeated runs of postselection. The theory line can be calculated straightforwardly, assuming that the state is Gaussian (fitted to the measured covariance matrix) and that the postselection filter is ideal (i.e., infinite cutoff). The data points show positive bias relative to the theory model, which correspond to deviations from normality due to experimental imperfections and to the nonideal filter implementation [Eq. (21)]. (a) Both measures increase with decreasing probability of success, but only logarithmic negativity surpassed the deterministic bound. (b) All of the measures in this figure lie below their respective deterministic bounds. The distillable entanglement is bounded from above by the relative entropy of entanglement, and this is represented by the orange region; in the case of the deterministic bound, the two measures coincide (represented by the overlaying orange and rose-colored dashed lines).

0% (Fig. 6). For each loss, the maximum gain g for the postselection filter was set to 1.6, 1.4, and 1.28, respectively, with unity gain corresponding to no postselection. We make the Gaussian assumption and infer the effective quantum state conditioned on successful postselection by calculating the covariance matrix of the postprocessed data. The cutoff for the filter was chosen to be large enough to justify the Gaussian assumption to at least 95% using the Jarque-Bera test of normality, which is based on skewness and kurtosis (the third and fourth moments). The entanglement measures may finally be evaluated on these effective states. We remark that different values of loss played different roles—a large amount of loss (90%) draws a clear distinction between logarithmic negativity and the other entanglement measures, a moderate amount of loss (50%) highlights the directionality of EPR steering and of coherent information, and a minimal amount of loss (0%) allows us to certify an increase in the distillable entanglement.

In Figs. 5 and 8, all measures indicate increasing entanglement with decreasing probability of success, as they should. What is perhaps more interesting is a comparison with the deterministic bound—that is, the maximum entanglement that can be transmitted through the channel in a deterministic fashion using an EPR resource with infinite squeezing. The resulting state is known as the Choi state of the channel [73]. We note that the deterministic bound is measure dependent, corresponding to the values of each measure evaluated on the Choi state. In Fig. 5(a), we see that logarithmic negativity crosses its deterministic bound at a relatively large probability of success, whereas the other measures will also cross their respective bounds but at much lower probabilities. The entanglement of formation was particularly far away from the bound even at the small success probability of 10^{-6}, although it can in principle cross the bound at sufficiently low probabilities of success [15]. We attribute this discrepancy to the operational meanings of the measures. The entanglement of formation measures the squeezing operations needed to produce an entangled state, while the logarithmic negativity is related to local squeezing that can be extracted from the state. The deterministic bound corresponds to a state for which a lot of squeezing is needed to produce it, but not much can be extracted from it; thus possessing a large entanglement of formation but a lower logarithmic negativity.

Results for the relative entropy of entanglement, for the squashed entanglement, and for the distillable entanglement are shown in Fig. 5(b). We approximate the relative entropy of entanglement using its Gaussian version (as explained in Sec. III F), numerically performing the minimization of Eq. (16) over separable two-mode Gaussian states. This approximation works relatively well when there is a large amount of loss (Fig. 7). Finally, the deterministic bound can be calculated analytically [58], and one finds that the relative entropy of entanglement does not cross the deterministic bound. We emphasize that the effects of noiseless linear amplification—the increase in squeezing and the reduction of loss [67]—guarantees that any measure must cross the bound at sufficiently small probabilities of success. However, the value of the probability of success might be too small to be accessed in the experiment, which is the case here.

Another important point to note for Fig. 5(b) is that the deterministic bound for the relative entropy of entanglement coincides with the bound for the distillable entanglement [58].

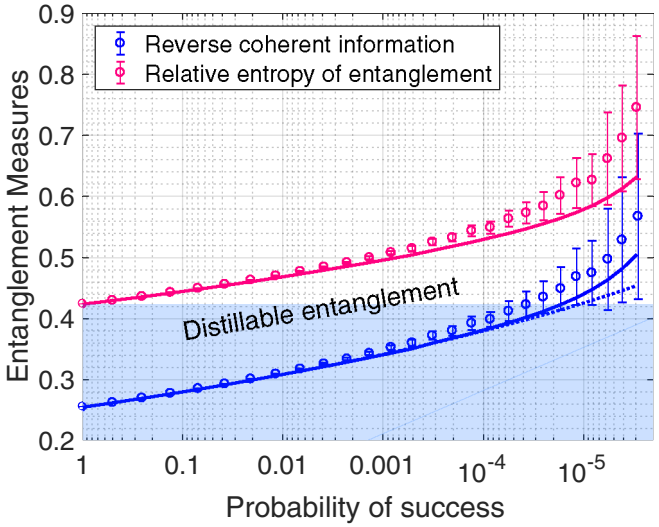

FIG. 6. Demonstrating an increase in the distillable entanglement. The loss was set to 0%. The distillable entanglement is bounded from above and from below by the relative entropy of entanglement and the reverse coherent information, respectively. The boundary of the blue shaded region is a horizontal line corresponding to the relative entropy of entanglement at unity probability of success, and values of the reverse coherent information lying above this line imply an increase in the distillable entanglement. The theory lines (given by the solid lines) in this figure assumes a finite cutoff, with the case of infinite cutoff also calculated for the reverse coherent information (dotted line), showing that its values are smaller but remains outside the blue region at small probabilities of success.

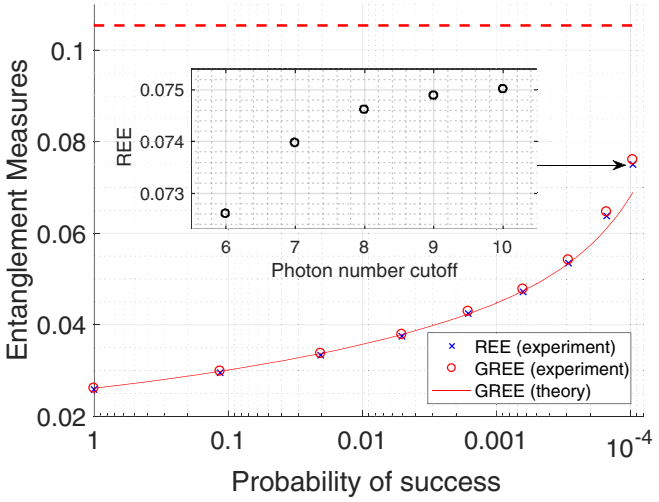

FIG. 7. A comparison of the relative entropy of entanglement and its Gaussian approximation. Inset shows the convergence of the numerical optimization for the relative entropy of entanglement as a function of the photon number cutoff; the cutoff is necessary as we are approximating a continuous-variable system using a finite-dimensional density matrix. The loss was set to 90%, and in such a case we find the two measures to be almost indistinguishable.

This is a useful fact for showing that the distillable entanglement does not cross the bound either. Although we cannot calculate the distillable entanglement directly (for general states other than the Choi state), we can bound it from above using the relative entropy of entanglement, as illustrated by the orange-shaded region in Fig. 5(b). This region lies below the deterministic bound, thus demonstrating that the distillable entanglement does not cross the bound.

We stress that the logarithmic negativity and the entanglement of formation are unable to provide evidence of this, despite being upper bounds of the distillable entanglement like the relative entropy of entanglement is. Both measures cross the deterministic bound *that is given by the distillable entanglement*, which one can read off Fig. 5(b) to be approximately 0.1 in value; thus these measures are unable to rule out the possibility that the distillable entanglement *could have* crossed the deterministic bound. As we have discussed in the previous paragraph, this cannot be true because the distillable entanglement is always less than the relative entropy of entanglement, which is in turn less than the deterministic bound of the distillable entanglement. The conclusion that the distillable entanglement did not cross the deterministic bound can only be drawn using the relative entropy of entanglement as the upper bound.

Figure 5(b) also shows results for squashed entanglement. Squashed entanglement is one of the measures for which there exist no convenient methods for calculating it; at best, we have a handful of bounds. For the case of two-mode Gaussian states, one of the best-known bounds is given in Ref. [59]; it can be evaluated for arbitrary phase-insensitive Gaussian channels and hence for states of the form Eq. (5) but not for those in the general form of Eq. (2). We note that such a requirement can be addressed by simply averaging the correlations of the amplitude and the phase quadratures, which are sufficiently close for the two-mode squeezed state generated in this experiment. As shown in Fig. 5(b), squashed entanglement does not cross the bound; however, one should keep in mind that the values for the squashed entanglement are approximations in the form of an upper bound and not the actual value of the measure itself.

We pause briefly to discuss the significance of the collective results in Fig. 5. The crossing of the deterministic bound by the logarithmic negativity suggests that the distilled state is better than the Choi state (i.e., an EPR state with *infinite* squeezing transmitted through the same communication channel). The possibility of doing better than the Choi state is certainly not forbidden by the laws of quantum mechanics and can, for instance, be achieved by using the noiseless linear amplifier with very large gains [67]. Nonetheless, we found that the logarithmic negativity has apparently "jumped the gun"—it suggests that this has already been achieved in the present experiment when all the other measures indicate otherwise. Thus, we have demonstrated a drawback for using the logarithmic negativity as the figure of merit, which is perhaps the price that one has to pay since it can be calculated so trivially.

Returning to the analysis, we consider the distillable entanglement in Fig. 6. It is similar to squashed entanglement in the sense that neither can be evaluated using straightforward means, but they differ because some of the bounds on the distillable entanglement are rather stringent [58]. We employ these stringent upper and lower bounds on the distillable

entanglement to demonstrate an increase in this quantity in the case of the lossless channel. We note that such a task would have been trivial if we knew how to calculate the measure—the need for using bounds in the case of the distillable entanglement is precisely because there is no method for calculating it directly.

Similarly to Refs. [16,17], we use the reverse coherent information to bound the distillable entanglement from below; however, we use the relative entropy of entanglement instead to bound it from above (as opposed to using the logarithmic negativity in Refs. [16,17]). If, after performing the entanglement distillation, the reverse coherent information ends up greater than the relative entropy of entanglement that we had started off with (indicated by the orange shading in Fig. 6), one may conclude that the distillable entanglement has increased. If the reverse coherent information remains smaller, then no conclusion can be drawn (corresponding to the blue shading). Figure 6 shows values of the reverse coherent information surpassing the bound given by the relative entropy of entanglement at low probabilities of success and hence an increase in the distillable entanglement. We remark that these results are fundamentally limited by state preparation and measurements—it cannot be improved simply by adjusting the postselection settings, due to excess noise and to the diminishing probability of success. In addition, the upper bound and the channel transmissivity cannot be arbitrary. There are other choices for the upper bound (Sec. III B), and one can also consider other settings for the loss (anything between 0% and 100%); however, no increase in the distillable entanglement was observed in any of these cases using the method presented above. In this sense, the results in Fig. 6 is optimal.

Adding to the collection, we consider relatives of entanglement measures. These are not proper entanglement measures in the axiomatic sense. Figure 8(a) illustrates the inseparability criteria for two-mode Gaussian states; the sum criterion [13] displays similar behavior to the PPT criterion, as both measures deal with the extraction of squeezing from entangled states [74]. The sum criterion relies on an extraction protocol that is suboptimal compared to the PPT criterion, and hence its values are closer to the separable boundary. Both are, of course, equally valid for certifying inseparability.

In Fig. 8(b) we show the results for EPR steering, a directional quantity for which the properties depend on the direction of interest. Reverse steering is particularly susceptible to loss, where an entangled state transmitted through 50% of loss would not be steerable in the reverse direction. It is interesting to note that, for this particular case, violation of the EPR steering criterion is equivalent to surpassing the deterministic bound. This is not true in general. By performing noiseless linear amplification, one is able to recover reverse steering beyond the deterministic bound at reasonable success probabilities, and one may compare this with forward steering—the deterministic bound is smaller to begin with and is also much harder to beat. Reverse steering is sensitive to loss because one is trying to steer using the lossy mode—most of the information about the entangled state has already been lost to the environment. In the case of direct steering, there is an advantage since one is using the mode that does not suffer from the loss of the channel.

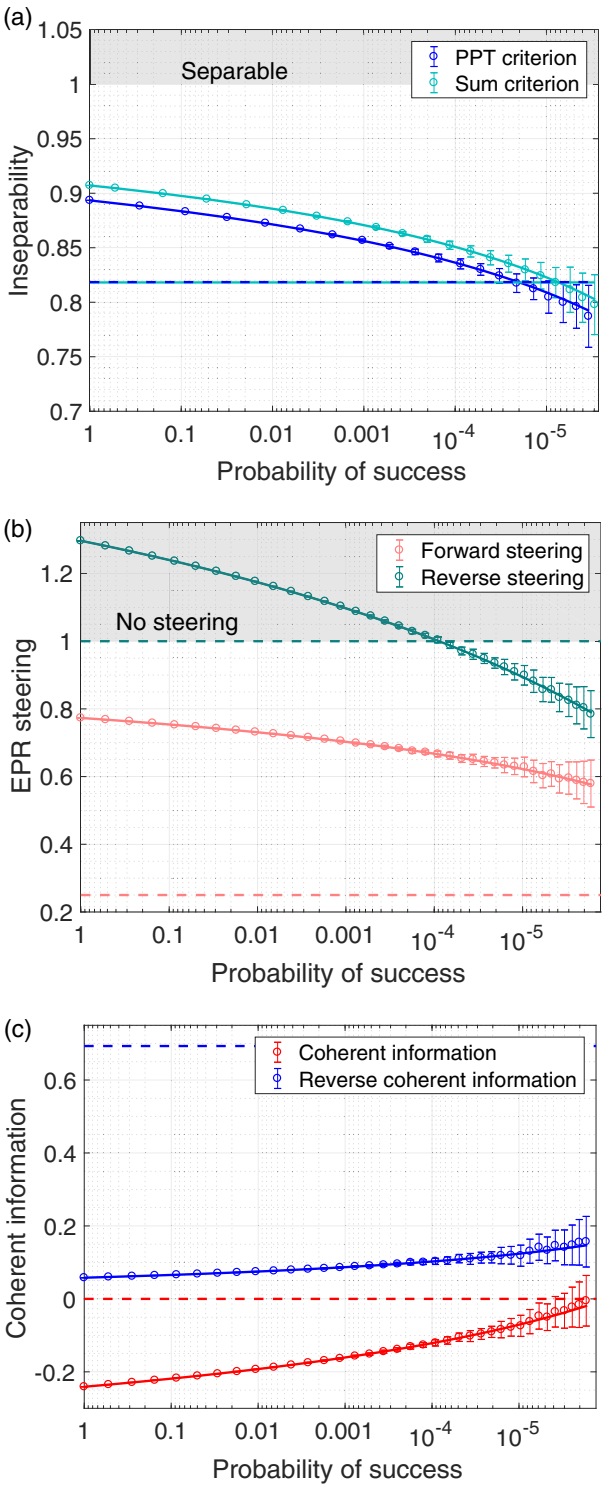

FIG. 8. Relatives of entanglement measures. The loss in (a) was set to 90%, while that in (b) and (c) is 50%. The data points (from top: sum criterion, PPT criterion, reverse steering, forward steering, reverse coherent information, coherent information), theory lines, deterministic bounds (from top: sum criterion and PPT criterion superimposed, reverse steering, forward steering, reverse coherent information, coherent information), and the error bars should be interpreted in the same way as those for Fig. 5. Noiseless linear amplification is useful for recovering forward steering and coherent information but less so for the other direction which is more robust to loss.

Finally, we consider the coherent information and the reverse coherent information, which are related to entanglement through the hashing inequality [Eq. (20)]. The reverse coherent information is robust against loss for the same reason that direct steering is; likewise, the coherent information is fragile the same way reverse steering is susceptible to loss [Fig. 8(c)]. The reverse coherent information is always positive even when no noiseless linear amplification was performed, while the coherent information was not initially positive but could be recovered at some small probability of success that is just out of reach in this experiment. Due to the robustness of the reverse coherent information, the deterministic bound is much harder to surpass.

V. CONCLUSION

By analyzing a measurement-based entanglement distillation experiment using a collection of measures, we showed that the logarithmic negativity exhibits behavior quite distinct from the others. It would make us believe that more entanglement has been distilled than what is offered by the deterministic bound, in stark contrast to what the other measures suggest. In addition to this result, we were also able to certify an increase in the distillable entanglement (in the case of the lossless channel), relying primarily on a judicious choice of the upper bound in order to estimate this quantity accurately. The work we have presented is useful for analyzing entanglement distillation but can also be extended to more general situations; this includes entanglement swapping, for instance, and the analysis of quantum repeaters in general.

ACKNOWLEDGMENTS

This work is supported by the Australian Research Council (ARC) under the Centre of Excellence for Quantum Computation and Communication Technology (Grants No. CE110001027, No. CE170100012, and No. FL150100019).

[1] N. C. Menicucci, P. van Loock, M. Gu, C. Weedbrook, T. C. Ralph, and M. A. Nielsen, Phys. Rev. Lett. **97**, 110501 (2006).
[2] V. Scarani, H. Bechmann-Pasquinucci, N. J. Cerf, M. Dusek, N. Lutkenhaus, and M. Peev, Rev. Mod. Phys. **81**, 1301 (2009).
[3] H. Takahashi, J. S. Neergaard-Nielsen, M. Takeuchi, M. Takeoka, K. Hayasaka, A. Furusawa, and M. Sasaki, Nat. Photon. **4**, 178 (2010).
[4] Y. Kurochkin, A. S. Prasad, and A. I. Lvovsky, Phys. Rev. Lett. **112**, 070402 (2014).
[5] H. M. Chrzanowski, N. Walk, S. M. Assad, J. Janousek, S. Hosseini, T. C. Ralph, T. Symul, and P. K. Lam, Nat. Photon. **8**, 333 (2014).
[6] A. E. Ulanov, I. A. Fedorov, A. A. Pushkina, Y. V. Kurochkin, T. C. Ralph, and A. I. Lvovsky, Nat. Photon. **9**, 764 (2015).
[7] J.-W. Pan, S. Gasparoni, R. Ursin, G. Weihs, and A. Zeilinger, Nature **423**, 417 (2003).
[8] P. G. Kwiat, S. Barraza-Lopez, A. Stefanov, and N. Gisin, Nature **409**, 1014 (2001).
[9] J. S. Bell, *Speakable and Unspeakable in Quantum Mechanics*, 2nd ed. (Cambridge University Press, Cambridge, England, 2004), pp. 37 and 198.
[10] O. Thearle, J. Janousek, S. Armstrong, S. Hosseini, M. Schünemann (Mraz), S. Assad, T. Symul, M. R. James, E. Huntington, T. C. Ralph, and P. K. Lam, Phys. Rev. Lett. **120**, 040406 (2018).
[11] T. C. Ralph, W. J. Munro, and R. E. S. Polkinghorne, Phys. Rev. Lett. **85**, 2035 (2000).
[12] R. Simon, Phys. Rev. Lett. **84**, 2726 (2000).
[13] L.-M. Duan, G. Giedke, J. I. Cirac, and P. Zoller, Phys. Rev. Lett. **84**, 2722 (2000).
[14] G. Vidal and R. F. Werner, Phys. Rev. A **65**, 032314 (2002).
[15] S. Tserkis, J. Dias, and T. C. Ralph, Phys. Rev. A **98**, 052335 (2018).
[16] R. Dong, M. Lassen, J. Heersink, C. Marquardt, R. Filip, G. Leuchs, and U. L. Andersen, Phys. Rev. A **82**, 012312 (2010).
[17] R. Dong, M. Lassen, J. Heersink, C. Marquardt, R. Filip, G. Leuchs, and U. L. Andersen, Nat. Phys. **4**, 919 (2008).
[18] C. Weedbrook, S. Pirandola, R. Garcia-Patron, N. J. Cerf, T. C. Ralph, J. H. Shapiro, and S. Lloyd, Rev. Mod. Phys. **84**, 621 (2012).
[19] R. Ukai, Multi-step Multi-Input One-Way Quantum Information Processing with Spatial and Temporal Modes of Light, Ph.D. thesis, The University of Tokyo, 2015.
[20] J. Williamson, Am. J. Math. **58**, 141 (1936).
[21] Y. Huang, New J. Phys. **16**, 033027 (2014).
[22] C. H. Bennett, H. J. Bernstein, S. Popescu, and B. Schumacher, Phys. Rev. A **53**, 2046 (1996).
[23] R. Horodecki, P. Horodecki, M. Horodecki, and K. Horodecki, Rev. Mod. Phys. **81**, 865 (2009).
[24] P. M. Hayden, M. Horodecki, and B. M. Terhal, J. Phys. A **34**, 6891 (2001).
[25] H. Araki and E. H. Lieb, Commun. Math. Phys. **18**, 160 (1970).
[26] M. M. Wilde, Phys. Rev. A **98**, 042338 (2018).
[27] C. H. Bennett, D. P. DiVincenzo, J. A. Smolin, and W. K. Wootters, Phys. Rev. A **54**, 3824 (1996).
[28] V. Vedral and M. B. Plenio, Phys. Rev. A **57**, 1619 (1998).
[29] M. Christandl and A. Winter, J. Math. Phys. **45**, 829 (2004).
[30] I. Devetak and A. Winter, Proc. R. Soc. A **461**, 207 (2005).
[31] Y. Akbari-Kourbolagh and H. Alijanzadeh-Boura, Quant. Info. Proc. **14**, 4179 (2015).
[32] J. S. Ivan and R. Simon, arXiv:0808.1658.
[33] G. Giedke, M. M. Wolf, O. Kruger, R. F. Werner, and J. I. Cirac, Phys. Rev. Lett. **91**, 107901 (2003).
[34] P. Marian and T. A. Marian, Phys. Rev. Lett. **101**, 220403 (2008).
[35] S. Tserkis and T. C. Ralph, Phys. Rev. A **96**, 062338 (2017).
[36] J. Hoelscher-Obermaier and P. van Loock, Phys. Rev. A **83**, 012319 (2011).
[37] N. J. Cerf, M. Levy, and G. Van Assche, Phys. Rev. A **63**, 052311 (2001).
[38] M. M. Wolf, G. Giedke, O. Kruger, R. F. Werner, and J. I. Cirac, Phys. Rev. A **69**, 052320 (2004).
[39] G. Adesso and F. Illuminati, Phys. Rev. A **72**, 032334 (2005).
[40] A. Peres, Phys. Rev. Lett. **77**, 1413 (1996).

[41] P. Horodecki, Phys. Lett. A **232**, 333 (1997).
[42] K. Audenaert, M. B. Plenio, and J. Eisert, Phys. Rev. Lett. **90**, 027901 (2003).
[43] S. Virmani and M. B. Plenio, Phys. Lett. A **268**, 31 (2000).
[44] A. Einstein, B. Podolsky, and N. Rosen, Phys. Rev. **47**, 777 (1935).
[45] E. Schrödinger, Camb. Phil. Soc. **31**, 555 (1935).
[46] E. Schrödinger, Camb. Phil. Soc. **32**, 446 (1936).
[47] M. D. Reid, Phys. Rev. A **40**, 913 (1989).
[48] W. P. Bowen, R. Schnabel, P. K. Lam, and T. C. Ralph, Phys. Rev. A **69**, 012304 (2004).
[49] H. M. Wiseman, S. J. Jones, and A. C. Doherty, Phys. Rev. Lett. **98**, 140402 (2007).
[50] V. Vedral, M. B. Plenio, M. A. Rippin, and P. L. Knight, Phys. Rev. Lett. **78**, 2275 (1997).
[51] C. Branciard, E. G. Cavalcanti, S. P. Walborn, V. Scarani, and H. M. Wiseman, Phys. Rev. A **85**, 010301 (2012).
[52] N. Walk, S. Hosseini, J. Geng, O. Thearle, J. Y. Haw, S. Armstrong, S. M. Assad, J. Janousek, T. C. Ralph, T. Symul, H. M. Wiseman, and P. K. Lam, Optica **3**, 634 (2016).
[53] S. Scheel and D.-G. Welsch, Phys. Rev. A **64**, 063811 (2001).
[54] X.-Y. Chen, Phys. Rev. A **71**, 062320 (2005).
[55] S.-J. Wu, Q. Wu, and Y.-D. Zhang, Chin. Phys. Lett. **18**, 160 (2001).
[56] S. Friedland and G. Gour, J. Math. Phys. **52**, 052201 (2011).
[57] Y. Zinchenko, S. Friedland, and G. Gour, Phys. Rev. A **82**, 052336 (2010).
[58] S. Pirandola, R. Laurenza, C. Ottaviani, and L. Banchi, Nat. Commun. **8**, 15043 (2017).
[59] K. Goodenough, D. Elkouss, and S. Wehner, New J. Phys. **18**, 063005 (2016).
[60] M. Takeoka, S. Guha, and M. M. Wilde, Nat. Commun. **5**, 5325 (2014).
[61] B. Schumacher and M. A. Nielsen, Phys. Rev. A **54**, 2629 (1996).
[62] I. Devetak, M. Junge, C. King, and M. B. Ruskai, Commun. Math. Phys. **266**, 37 (2006).
[63] R. Garcia-Patron, S. Pirandola, S. Lloyd, and J. H. Shapiro, Phys. Rev. Lett. **102**, 210501 (2009).
[64] H. Ollivier and W. H. Zurek, Phys. Rev. Lett. **88**, 017901 (2001).
[65] M. Idel, D. Lercher, and M. W. Wolf, J. Phys. A: Math. Theor. **49**, 445304 (2016).
[66] K. C. Tan, T. Volkoff, H. Kwon, and H. Jeong, Phys. Rev. Lett. **119**, 190405 (2017).
[67] T. C. Ralph and A. P. Lund, in *Quantum Communication Measurement and Computing Proceedings of 9th International Conference*, edited by A. Lvovsky (AIP, New York, 2009), pp. 155–160.
[68] J. Fiurasek, Phys. Rev. A **80**, 053822 (2009).
[69] C. Caves, Phys. Rev. D **26**, 1817 (1982).
[70] G. Y. Xiang, T. C. Ralph, A. P. Lund, N. Walk, and G. J. Pryde, Nat. Photon. **4**, 316 (2010).
[71] J. Fiurasek and N. J. Cerf, Phys. Rev. A **86**, 060302 (2012).
[72] J. Zhao, J. Y. Haw, T. Symul, P. K. Lam, and S. M. Assad, Phys. Rev. A **96**, 012319 (2017).
[73] M.-D. Choi, Linear Algebra Appl. **10**, 285 (1975).
[74] V. Giovannetti, S. Mancini, D. Vitali, and P. Tombesi, Phys. Rev. A **67**, 022320 (2003).